

One-step green synthesis of TiO₂-Ag nanocomposites and their performance towards photocatalytic activities and antimicrobial properties

Sunderishwary S. Muniandy^a, Shueai Tan^a, Noor Haida Mohd Kaus^b, S. Sasidharan^c, Hooi Ling Lee^{a*}

^aNanomaterials Research Group, School of Chemical Sciences, Universiti Sains Malaysia, 11800 Penang, Malaysia., ^bNano Hybrid Materials Group, School of Chemical Sciences, Universiti Sains Malaysia, 11800 Penang, Malaysia., ^cInstitute for Research in Molecular Medicine (INFORMM), University Sains Malaysia, 11800 Penang, Malaysia

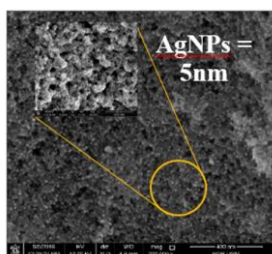
*Corresponding Author: hllee@usm.my

Article history :

Received 21 January 2017

Accepted 8 March 2017

GRAPHICAL ABSTRACT



ABSTRACT

Heterogeneous nanocomposites consist of metal oxide and noble metals such as titanium dioxide (TiO₂)-silver (Ag) are explored extensively using various methods. In the current work, TiO₂-Ag nanocomposites (NCs) were prepared using facile hydrothermal technique. The nanocomposites were synthesised at 160 °C for 24 hours with titanium(IV) isopropoxide (TTIP), silver nitrate (AgNO₃) as precursors and polyvinylpyrrolidone (PVP) as a reducing agent. The sample with the best antibacterial and photocatalytic properties were further characterised by X-ray diffraction (XRD), nitrogen adsorption analysis (NAA) and field-emission scanning electron microscopy (FESEM). The as-synthesised TiO₂-Ag nanocomposites with different TTIP loading were tested on methylene blue (MB) under sunlight as well as antibacterial activities against Gram-positive bacteria (*Bacillus subtilis*) and Gram-negative bacteria (*Escherichia coli*). TiO₂-Ag nanocomposite showed two times broader zone of inhibition than AgNPs on both *Bacillus subtilis* (19.3 ± 0.57 mm) and *Escherichia coli* (25.3 ± 0.57 mm). This smart material with small Ag particles (5nm) decorated on compact aggregates of TiO₂ synthesised via green method has high potential in applications that combine both self-cleaning and antibacterial properties.

Keywords: Titanium dioxide, silver, green synthesis, nanocomposites

© 2017 Dept. of Chemistry, UTM. All rights reserved
| eISSN 0128-2581 |

1. INTRODUCTION

Nanocomposites have been attracting a great deal of interest for a variety applications ranging from packaging, automotive, electrical, biomedical and other properties due to their attractive mechanical properties and advanced physical properties such as thermal and electrical conductivities offered by different types of nanoparticles. Heterogeneous nanocomposites consisting of semiconductor and noble metals received the utmost attention compared to polymer/ceramic based nanocomposites because of its hybridisation of two or more materials with distinctive properties, which acts synergistically to develop new functionalities and improving their properties. In the past decades, hybridisation of metal oxide-metal materials such as Pt-TiO₂ [1], Pd-TiO₂ [2], Ag-TiO₂ [3-4], Au-TiO₂ [5], Fe₃O₄- Au/Pt/Pd [6], Pd-CeO₂ [7-9], and Ag-Mn₃O₄ were extensively studied to enhance the property of end product. However, numerous researches were more focused on improving single property of a material instead of focusing on the advantage of hybridisation in producing a material with dual functionalities.

The use of nanostructured inorganic materials with antibacterial properties has drawn considerable attention due to their higher heat resistance, lower decomposability, and longer life expectancy. Among inorganic nanomaterials,

metallic silver (Ag) has been known as effective antimicrobial agents because Ag is a noble metal that does not corrode under photocatalytic conditions [10]. For economical and efficient use of Ag, composite materials incorporating Ag nanoparticles have been developed and tested in diverse applications. However, agglomeration of Ag nanoparticles with composite material represents a major limitation as agglomerated particles have smaller surface area. A good dispersion of Ag particles together with the host materials is necessary for sufficient interaction between Ag and the composite material (synergistic effect) to meet the demands of practical applications [11]. Thus, a great deal of research was focused to produce well-dispersed, small (sub-10 nm) composite particles with high synergistic effect. To improve the synergy effect between Ag and composite materials, several strategies were adopted such as incorporating metal oxides with Ag particles and formation of nanocomposites with dual properties.

Herein, titanium dioxide (TiO₂) was selected to be incorporated with silver in order to produce a dual functionalised material, TiO₂-Ag nanocomposites (TiO₂-Ag NCs). Previous studies showed that TiO₂ can be an ideal candidate for integration with silver since the chemical and physical properties of both metal and metal oxide can be enhanced. TiO₂, a binary metal oxide with band gap of 3.2 eV for anatase. It has received large attention due to its

biological and chemical inertness, cost-effectiveness, low toxicity and ease of preparation in bulk or nanostructured forms [12]. In addition, TiO₂ semiconductor has been always regarded as one of the most promising photocatalysts in practical applications, especially water cleaning [13–16] and removal of volatile organic compounds (VOCs) in air [17–19], owing to its high photocatalytic property. Nowadays, visible light response is the disadvantage still yet to be overcome. In order to achieve efficient photocatalysts, solar light or interior lighting irradiations are employed. Hence, silver is coupled to TiO₂ in order to extend the light response in the solar or visible region [11]. According to a number of studies, results indicated that TiO₂-Ag nanocomposites may contain the advantages of both materials: silver has a higher antimicrobial activity, and TiO₂ can last longer, and able to be controlled by illumination.

Despite the abundant simultaneous efforts made to explore the metal oxide-metal nanocomposites for various applications and reports on the conventional synthesis, the synthesis of TiO₂-Ag nanocomposites using green approach was investigated only in a few reports [20–22]. The main objective of green technique is to avoid waste generation where different shades of greener processes are being introduced in conventional syntheses. Green chemistry approach is referred to explore alternative effective reaction conditions that utilise renewable resources wherever possible and environmentally benign reaction media to accomplish the desired chemical transformations with minimized by-products or waste, as well as eliminating the use of conventional organic solvents wherever possible. Several recent studies have been reported on the methods to synthesise TiO₂-Ag NCs. These include (i) sol-gel method [23–25] (ii) hydrothermal [26–28] (iii) using leaf extracts and [29,30] (iv) electrochemical deposition [31,32]. However, most of the methods employs harmful reagent, longer reaction time and requires complicated process. Therefore, altering an existing methods for synthesis of NCs by applying green chemistry principles is considered better and more advanced as it is eco-friendly, sustainable, and relatively reproducible and the end products are often more stable [33].

To meet these requirements, we designated a modified one-pot green method to prepare TiO₂-Ag nanocomposites using hydrothermal technique. Polyvinylpyrrolidone (PVP) serves as the reducing agent and stabilizers to control Ag cluster growth. The synthesis was carried out in water as reaction media with presence of titanium tetraisopropoxide (TTIP) and silver nitrate (AgNO₃) as the precursors. Potent antibacterial activity against *Escherichia coli* and *Bacillus subtilis*, a typical Gram negative and Gram positive bacterial strain respectively, has been achieved using this nanocomposite. Besides, the as-synthesised nanopowder was used as a heterogeneous catalyst against methylene blue (MB) solution under sunlight to explore their potential on photocatalytic activities.

2. EXPERIMENTS

2.1 Preparation of TiO₂-Ag NCs

The TiO₂ – Ag NCs nanopowders were synthesised with a facile hydrothermal method according to the work by Zhu, J. and the co-workers [34] with some modifications. In a typical procedure, 1 mL (0.0364 M) of tetraisopropoxide (TTIP) was added into 50 mL distilled water under magnetic stirring. Then, 0.612 g of silver nitrate (AgNO₃) and 0.4 g polyvinylpyrrolidone (PVP) were dissolved, respectively, in a 20 mL of distilled water. The molar ratio between the repeating unit of PVP and AgNO₃ was fixed at R = 1. Both solutions were simultaneously injected dropwise into the magnetically stirred TTIP solution. Constant magnetic stirring was applied for 15 minutes. The entire mixture was then transferred into a Teflon vessel (capacity = 100 mL), which was placed in a stainless steel hydrothermal reactor and heated at 160 °C for 24 h. For characterisations, the mixtures were sampled at different TTIP loading and was then washed and centrifuged repeatedly to remove possible contamination (excess PVP).

2.2. Characterisations

The crystallinity and phase purity of the synthesised photocatalyst was analysed by powder X-ray diffraction (XRD) (PW 3040/60 X'PERT PRO, PANalytical) using CuK_α (1.541 Å) radiation in the range 2θ = 10 – 90°. The specific surface area and pore size distribution studies were measured by nitrogen adsorption isotherms using a N₂ adsorption analyser (NAA) (Micromeritics ASAP 2020 Surface Adsorption Porosimeter (SAP)). Pore size distributions and pore volumes were determined from the sorption isotherms using the Brunauer-Emmett-Teller (BET) and Barrett-Joyner-Halenda (BJH). The morphology of the as-prepared photocatalyst powder was characterised by field emission scanning electron microscope (FESEM) (Leo Supra 50 VP Field Emission SEM). An acceleration electron voltage of 10kV voltage was applied to obtain the FESEM images.

2.3. Photocatalytic test on methylene blue (MB) dye

Photocatalytic activities of TiO₂-Ag NCs were evaluated by degradation of methylene blue (MB) solution under sunlight irradiation. The experiment was performed using 0.1 g of catalyst in 200 mL of 6 mg/l MB solution under continuous shaking for one hour in (dark) and then exposed to sunlight (75 – 120 kLux) for two hours. In this experiment, samples were collected for every 15 minutes during photocatalysis were centrifuged to separate TiO₂-Ag particles from MB solution before analysed using UV-vis spectrometer (LAMBDA 25 UV/Vis Systems). The removal efficiency of MB solution can be calculated using the following equation:

$$R = \frac{(C_0 - C_t)}{C_0} \times 100 \% \quad (1)$$

where C_0 is the initial concentration of MB solution and C_t is concentration of MB solution during irradiation.

2.4 Antimicrobial activities of TiO₂-Ag NCs

The antimicrobial test of TiO₂-Ag NCs were quantitatively conducted by the bacterial inhibition ring method (agar plate disc diffusion assay) against Gram-negative bacterium *Escherichia coli* (*E. coli*) and Gram-positive bacterium *Bacillus subtilis* (*B. subtilis*). Nutrient agar medium was prepared by Mueller-Hinton (MH) agar culture medium (HiMedia, Mumbai, India) in 1 L distilled water at pH 7.2. The agar medium and empty Petri plates were autoclaved for sterilisation purpose. Then, the agar medium was then cast into the Petri plates and cooled down [35]. The samples were inoculated in Petri dishes with MH medium agar and then paper disks of 5 mm in diameter were planted on the inoculated test organism agar at equidistant spots. Diluted solution (30 µg/ml) of TiO₂-Ag NCs synthesised using different TTIP loading were instilled (20 µl) on the inoculated disc and left for 10 min at room temperature for the compound diffusion. Chloramphenicol (30 µg/ml) was used as the control for the antimicrobial test. The plates inoculated with bacteria and samples were incubated at 37 °C for 24 hours. The presence of clear zone around the discs, also known as zone of inhibition (ZOI) on the plates was recorded as an inhibition against the microbial species. The mean and standard deviation reported for each type of NC and each microbial strain were tested in triplicate.

3. RESULTS AND DISCUSSION

3.1 XRD analysis

Powder X-ray diffraction (XRD) analysis of the crystalline TiO₂-Ag NCs sample prepared using 1 mL, 3 mL and 5 mL of TTIP, presented in Fig 1 shows the presence of anatase, brookite and silver peaks. Peaks labelled as circle and square correspond to anatase and brookite phases, respectively. The XRD patterns obtained from calcined and uncalcined samples display similar characteristics which exhibited reflection characteristics at 2θ of 25.7°, 38.3°, 48.4°, 55.4° and 77.5° corresponding to (101), (004), (200), (105), and (204) planes of the anatase phase, respectively. This figure also clearly showed reflection characteristics at of the (210) diffraction peak located at 30.9° equivalent to the brookite phase. It is necessary to take into account that the main (101) diffraction peak of anatase at $2\theta = 25.7^\circ$ overlaps with the (120) and (111) peaks of brookite at $2\theta = 25.34^\circ$ and 25.69° , respectively, where the sample have a mixture of anatase and brookite. However, the peak of anatase at $2\theta = 62.57^\circ$, which did not overlap with any diffraction peak of brookite confirmed the existence of

anatase phase [36]. The transformation of anatase to brookite can be explained by the fact that under the present conditions brookite displayed a higher thermal stability than anatase and thus, brookite particles can act as nucleation sites for the anatase to brookite transformation [37]. The reflections at 38.3°, 44.5° and 64.4° represented (111), (200) and (220) planes of the face-centered phase of silver metal. It should also be noted that the peak of the (111) plane is more intense than those of other two peaks, suggesting strong growth network of AgNPs are enclosed with the (111) plane [38]. An apparent decrease and broadening of Ag peak intensity can be seen after the calcination process, indicated that Ag nanoparticles probably have been introduced into the pore channels or due to the size contraction of the Ag nuclei may cause reduction of the peak intensity [39]. Indeed, these results demonstrated that small Ag nanoparticles were mounted and dispersed on the TiO₂ particles [40]. The peak positions presented by the diffraction patterns were all in accordance with those given in PDF card 98-010-5399 for anatase phase, PDF 98-008-3898 for Ag, PDF 98-001-6988 for brookite phase.

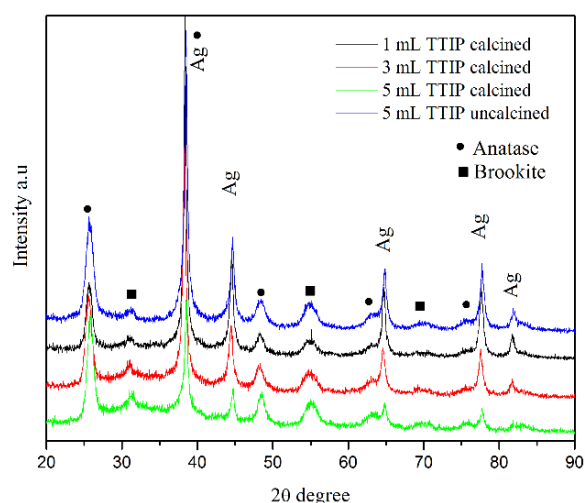


Fig. 1 XRD patterns for the 1 mL TTIP, 3 mL TTIP, 5 mL TTIP calcined and 5 mL TTIP uncalcined of synthesised TiO₂-Ag

3.2 Structures and morphology

Four different TTIP loading, 0.0364 M (1 mL), 0.1092 M (3 mL), 0.1819 M (5 mL) and 0.1819 M uncalcined, were selected for the FESEM observation. From Fig. 3 (a) - (c), it was observed that the particle size decreased as the TTIP loading increased. Fig. 3 (b) and (c) present a numerous small particles of TiO₂ and Ag compared to Fig. 3 (a) where the structure of TiO₂ particles with small spherical Ag nanoparticles (white spots) can be seen clearly. Considering that heavy elements (e.g. Ag) backscattered electrons more strongly than light elements (e.g. O, Ti), the metallic silver appears brighter in the image [41]. Thus, the brighter Ag nanoparticles with a diameter around 5 nm were well dispersed in Fig. 3 (a) - (c). The reduced size of the Ag clusters may be related to the effect of confined electrons.

This phenomenon can be related with electronic barrier sets [49] for Ag NPs with very small sizes, diameters < 20 nm. Conversely, the sample prepared using 5 mL of TTIP without calcinations shows isolated large Ag particles on the surface of TiO₂ particles. Here, we can conclude that the calcination process leads to size reduction in Ag particles. Large particles were observed for the sample synthesised with low TTIP loading. This is because of increase in particle growth as the precursor concentration decreases, and therefore, large primary particles are produced under solute with low precursor concentration. As the TTIP loading increased, extremely small particles were produced. This phenomena occurred due to dense solute presents a reduced volume, and compact aggregates occur with strong attraction between particles which built up a compact aggregate of small nanoparticles [42].

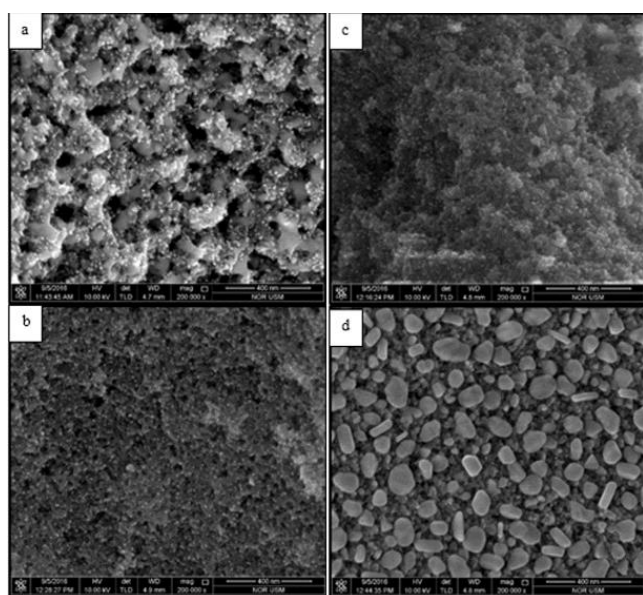


Fig. 2 FESEM images of the TiO₂- Ag NCs synthesised using (a) 1 mL TTIP (b) 3 mL TTIP (c) 5 mL TTIP (d) 5 mL TTIP uncalcined

3.3 NAA and BET analysis

The representative (a) N₂ adsorption/desorption isotherms and the (b) Barrett–Joyner–Halenda (BJH) pore size distribution profiles of calcined samples with different TTIP loadings and uncalcined TiO₂-Ag NCs shown in Fig. 2. All the sample exhibited type IV nitrogen isotherm with H1 loop implying the presence of mesopores at high relative pressure range between 0.6 and 0.9 [43]. H1 hysteresis loop typically implies that the as-synthesised samples with consist of agglomerates or compacts of approximately uniform spheres in fairly regular array with high degree of pore size uniformity [44]. It can be seen from Figure 3(a) that the adsorption for the uncalcined sample synthesised using 5 mL TTIP was completed at a relative pressure of 0.6. However, the monolayer adsorption for calcined samples was incomplete until it reaches a relative pressure of 0.8. This indicates that mesoporous uncalcined sample possesses

much smaller pore size than the calcined samples. Moreover, the N₂ adsorption quantity for the sample prepared without calcination is much higher than that of the calcined sample, representing the abundance of mesopores in the uncalcined TiO₂-Ag NCs. It is also interesting to note that BET specific surface areas, pore volumes, and average pore diameters also changed with the amount of TTIP used in preparation, as shown in Table 1. The BET specific surface areas increased and pore diameters decreased with the increasing amount of TTIP. Calcined sample prepared with 5 mL TTIP exhibited the highest BET surface area of 51.35 m²/g compared to calcined sample prepared using 1 mL (35.3 m²/g) and 3 mL (45.2 m²/g) TTIP.

Table 1 Surface area (S_{BET}), average pore diameters and kinetic parameters data for degradation of MB dye for TiO₂- Ag NCs samples synthesised using various TTIP loading.

TTIP loading	S_{BET} (m ² g ⁻¹)	Average pore diameters (nm)	k (min ⁻¹)	R ²	Degradation (%)
1 mL	35.3	31.5	0.026	0.992	100 (2 hours)
3 mL	45.2	18.8	0.035	0.992	100 (1h 45 min)
5 mL	51.7	15.3	0.042	0.987	100 (1h 15 min)
5 mL uncalcined	110.8	7.9	0.007	0.993	61.61 (2 hours)

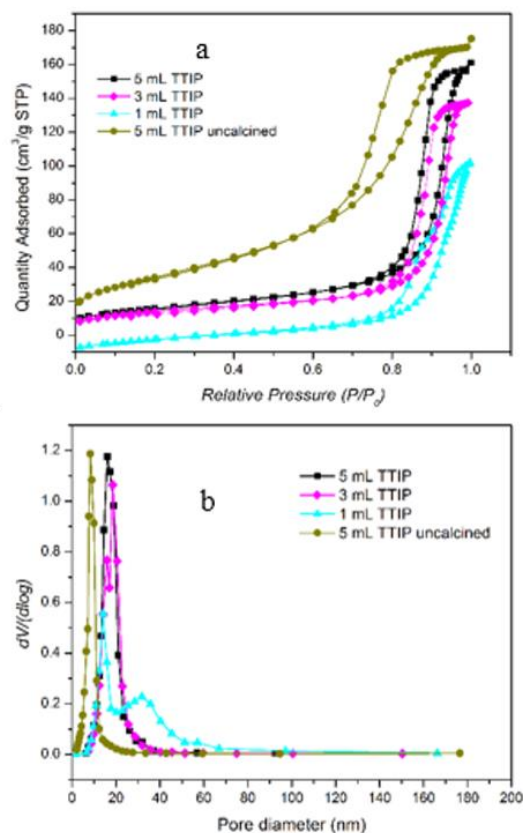


Fig. 3 (a) Nitrogen adsorption-desorption isotherm and (b) pore size distribution of synthesised TiO₂- Ag NCs (TTIP loadings: 1 mL, 3 mL, 5 mL and 5 mL uncalcined).

It showed a good agreement with FESEM micrographs, as the size of particles decreased drastically and lead to increase in surface area when the TTIP loading increased. However, uncalcined sample shows higher BET value which is 110.8 m²/g compared to calcined samples. This behavior can be linked to the removal of organic molecules after the heat treatment induced an increase in pores size and reduce the specific surface area [45]. The average pore diameter for calcined sample prepared using 5 mL TTIP increased drastically from 7.9 nm (5 mL TTIP uncalcined sample) to 15.3 nm. These larger pores are presumably formed by the aggregation of small mesoporous particles when calcination is performed. Also, it was verified that all the synthesised samples revealed higher BET surface area as compared to pure TiO₂ anatase nanopowder (10.4 m²/g) (purity ≥ 99% anatase; titanium (IV) oxide purchased from Sigma-Aldrich, USA).

3.4 Photocatalytic properties

The photocatalytic activity of TiO₂-Ag NCs powder was evaluated by degradation of methylene blue (MB) solution. Fig. 4 shows the photocatalytic activity of as-synthesised nanocomposites samples using various loading of TTIP against 6 mg/L MB solution. The results showed that when the loading of precursor (TTIP) increased from 0.0364 M (1 mL) to 0.1819 M (5 mL), the photocatalytic activities increased gradually. Compared with the uncalcined sample, the result showed that without calcination process only 61.61% of MB solution was degraded in two hours. The possible reason for this might be the polymer (PVP) partially covered the photocatalyst particles and interfered with the photocatalytic degradation of model pollutant [46]. When the loading of TTIP increased, the particle sizes were reduced extremely and directly increased the surface area of the sample which have been proven through FESEM micrographs and NAA analysis. Hence, the photocatalytic activity of TiO₂-Ag NCs against MB solution is favourable and enhanced as the TTIP loading increased.

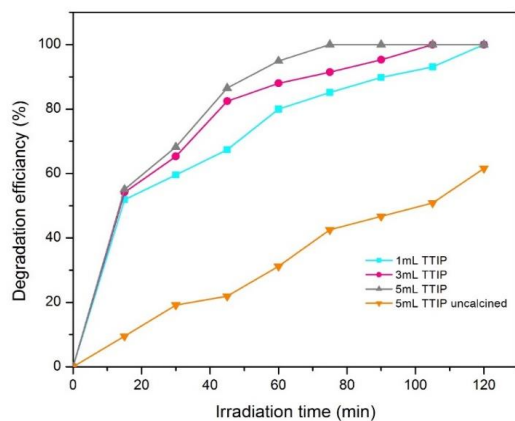


Fig. 4 Time profile of methylene blue degradation for TiO₂-Ag NCs obtained from different loading of TTIP.

The reaction rate constants, k (as shown in Table 1 and Fig. 5) are calculated according to the pseudo first-order model which is generally used for photocatalytic degradation process when the initial concentration of pollutant is low,

$$\ln\left(\frac{C_0}{C_t}\right) = kt \quad (2)$$

where C_0 and C_t are the concentrations of MB aqueous solution at irradiation times of 0 and t min, respectively.

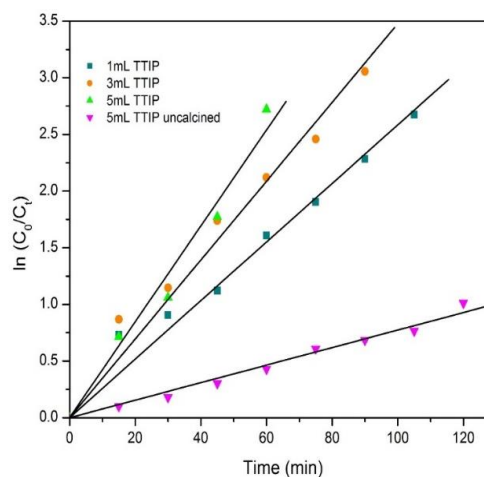


Fig. 5 Kinetic analyses for photodegradation of methylene blue dye for samples synthesised under different TTIP loading.

3.5 Antimicrobial activity of TiO₂-Ag NCs

The bactericide activity of TiO₂-Ag nanocomposites was evaluated in absence of light, through disc diffusion assay against Gram-negative bacteria *E. coli* and Gram-positive bacteria *B. subtilis*. A summary of positive results in Fig. 6 and Table 2 suggests that TiO₂-Ag nanopowders underwent an interaction with bacterial cell and displayed the strong action against *E. coli*, and *B. subtilis*. The antibacterial activity of TiO₂-Ag NCs against both bacteria increases strongly for the calcined samples compared to uncalcined samples. This is because removal of polymer through calcinations process provides a better availability for TiO₂-Ag NCs. Besides, antibacterial property for the nanocomposites worked two fold better than AgNPs because of the size reduction of Ag cluster on the surface of TiO₂ particles induces a higher extent for the synergy. Control tests were performed at these same concentrations of that tested for the nanocomposite to estimate the influence of pure TiO₂ on the bacteria growth inhibition.

E. coli bacteria were the most sensitive strain (Table 2) because it showed the highest antibacterial activity for all the samples. This is related the fact that they are Gram-negative bacteria and mainly could be vulnerable to ionic interactions with silver ions [47]. Despite some reports that have shown that Gram-negative bacteria more resistant toward nanocomposites, our results showed Gram-positive bacteria was more resistant towards synthesised samples.

This could attribute to the electronic confinement barriers of the sample can destroy the bacteria membrane by the penetration of extremely small TiO₂-Ag NCs, similar as reported by Z. Vineth and co-workers [48].

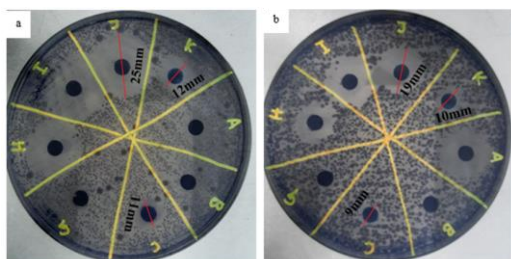


Fig. 6 Ring of inhibition of TiO₂-Ag NCs against (a) *E. coli* and (b) *B. Subtilis*

Table 2 Zone of inhibition of TiO₂-Ag NCs against *E. coli* and *B. Subtilis*

Samples	Average zon of inhibition (mm)	
	<i>E.coli</i>	<i>B. subtilis</i>
A(Cholaramphenicol)	10.3 ± 0.57	9.5 ± 0.57
B (PVP)	-	-
C (1:1 AgNP)	11.3 ± 0.57	9.3 ± 0.57
G (TiO ₂ NP)	-	-
H (1 mL TTIP)	20.7 ± 0.57	15.0 ± 1.0
I (3 mL TTIP)	25.3 ± 0.57	18.0 ± 0.57
J (5 mL TTIP)	25.3 ± 0.57	19.3 ± 0.57
K (5 mL TTIP uncalcined)	12.5 ± 1.5	10.3 ± 0.57

4. CONCLUSION

An alternative green method was used to synthesise TiO₂-Ag NCs by hydrothermal technique. TiO₂-Ag composite material with small Ag particles (5nm) decorated on compact aggregates of TiO₂ was successfully synthesised using titanium tetraisopropoxide (TTIP) and silver nitrate (AgNO₃) as the precursors, water as the solvent, and polyvinylpyrrolidone (PVP) as the stabiliser or reducing agent. Corroborative results from FESEM, XRD and NAA revealed the composition and crystalline structure of the composite, as well as the size and distribution of the Ag nanoparticles on the TiO₂ particles. As-synthesised nanocomposite powder seems to promote photoactivity towards the MB solution under solar light and the results clearly indicated as the loading of TTIP increased, the particle size reduced and increased the surface area which contributed to better photocatalytic performance. This work also shows the synergistic relationship between silver and titanium dioxide and clearly indicates the link between the extent of the synergy and the size of the silver nanoparticles: a decrease of the nanoparticle size induces a higher extent for the synergy. This phenomena leads to better antimicrobial activities (two folds better than AgNPs) against Gram positive (*Bacillus subtilis*) and Gram negative (*Escherichia coli*). The method developed in this work is proven green and environmentally friendly for the preparation of TiO₂-Ag NCs powders with advantages of both material, photocatalytic and antimicrobial properties.

ACKNOWLEDGEMENTS

This work was financially supported by the USM Research University Individual Grant (RUI: 1001/PKimia/811265).

REFERENCES

- [1] J.J. Zou, C.J. Liu, K.L. Yu, D.G. Cheng, Y.P. Zhang, F. He, et al, Chem. Phys. Lett. 400 (2004) 520.
- [2] B. Tapin, F. Epron, C. Especel, B.K. Ly, C. Pinel, M. Besson, ACS Catal. 3 (2013) 2327.
- [3] D. Yang, Y. Sun, Z. Tong, Y. Tian, Y. Li, Z. Jiang, J. Phys. Chem. C. 119 (2015) 5827.
- [4] O. Akhavan, J. Colloid Interf. Sci. 336 (2009) 117.
- [5] S.C. Chan, M. Barteau, Langmuir. 21 (2005) 5588.
- [6] F. Lin, W. Chen, Y. H. Liao, R. Doong, Y. Li, Nano. Res. 3 (2011) 676.
- [7] L. Adjianto, D. A. Bennett, C. Chen, A. S. Yu, M. Cargnello, P. Fornasiero, et al., Nanotechnology Lett. 13 (2013) 2252.
- [8] H. Tan, J. Wang, S. Yu, K. Zhou, Environ. Sci. Technol. 49 (2015) 8675.
- [9] G. Li, L. Li, Y. Yuan, J. Shi, Y. Li, Y. Yuan, et al., Appl. Catal. B Environ. 158-159 (2014) 341.
- [10] A. Amarjargal, L.D. Tijjing, C.S. Kim, Dig. J. Nanomater. Biostructures. 6 (2011) 1957.
- [11] C.A. Castro, A. Jurado, D. Sissa, S.A. Giraldo, Int. J. Photoenergy. (2012) 1.
- [12] M. Pelaez, N. T. Nolan, S. C. Pillai, M. K. Seery, P. Falaras, A. G. Kontos, et al., Appl. Catal. B. Environ. 125 (2012) 331.
- [13] M. N. Chong, B. Jin, C. W. K. Chow, C. Saint, Water. Resour. Bull. 44 (2010) 2997.
- [14] M. J. Wu, T. Bak, P. J. O'Doherty, M. C. Moffitt, J. Nowotny, T. D. Bailey, et al., Int. J. Photochem. (2014) 1.
- [15] M. A. Lazar, S. Varghese, S. S. Nair, Catal. Lett. 2 (2012) 572.
- [16] F. Madjene, L. Aoudjit, S. Igoud, H. Lebig, B. Boutra, Transnat'l. J. Sci. Technology. 3 (2013) 34.
- [17] Y. Huang, S. S. H. Ho, R. Niu, L. Xu, Y. Lu, J. Cao, et al., Molecules. 21 (2016) 1.
- [18] L. Zou, Y. Luo, M. Hooper, E. Hu, Chem. Eng. Process. 45 (2006) 959.
- [19] Y. Huang, S. S. H. Ho, R. Niu, L. Xu, Y. Lu, J. Cao, et al., Molecules. 21 (2016) 1.
- [20] X. Lv, F. Gao, Y. Yang, T. Wang, Ind. Eng. Chem. Res. 55 (2016) 107.
- [21] J. Liu, I. Medina-ramirez, Z. Luo, S. Bashir, R. Mernaugh, A. Texas, et al., NSTI-Nanotech. 1 (2010) 1920.
- [22] K. Tahir, A. Ahmad, B. Li, S. Nazir, A. U. Khan, T. Nasir, et al., J. Photochem. Photobiol. B. Biol. 162 (2016) 189.
- [23] M. Epifani, C. Giannini, L. Tapfer, L. Vasanelli, J. Am. Ceram. Soc. 83 (2000) 2385.
- [24] M. Zainizan Sahdan, N. Nayan, S. Haimi Dahlan, M. E. Mahmoud, U. Hashim, Adv. Mater. Phys. Chem. 2 (2012) 16.
- [25] J. D. Lee, H. C. Kim, Y. S. Kim, Y. D. Kim, M. S. Lee, Solid State Phenom. 124 (2007) 1059.
- [26] P. Govindhan, C. Pragathiswaran, J Mater. Sci. Mater. Electron. 27 (2016) 8778.
- [27] C. Liu, D. Yang, Y. Jiao, Y. Tian, Y. Wang, Z. Jiang, ACS Appl. Mater. Interfaces. 5 (2013) 3824.
- [28] K. Kusdiant, D. Jiang, M. Kubo, M. Shimada, Ceram. Int. (2017) 1.
- [29] S. M. Roopan, A. Bharathi, A. Prabhakarn, A. Abdul Rahuman, K. Velayutham, G. Rajakumar, et al., Spectrochim. Acta - Part A Mol. Biomol. Spectrosc. 98 (2012) 86.
- [30] M. Atarod, M. Nasrollahzadeh, S. Mohammad Sajadi, J. Colloid. Interf. Sci. 462 (2016) 272.
- [31] S. Ashok Kumar, P. H. Lo, S. M. Chen, Nanotech. 19 (2008) 255.
- [32] M. M. Khan, S. A. Ansari, J. Lee, M. H. Cho, Mater. Sci. Eng. C. 33 (2013) 4692.

- [33] G. Zhang, X. Shen, Y. Yang, *J. Phys. Chem. C* 115 (2011) 7145.
- [34] G. H. Wang, J. J. Zhu, C. X. Kan, J. G. Wan, M. Han, *J. Nanomater.* (2011) 1.
- [35] M. Shateri Khalil-Abad, M. E. Yazdanshenas, *J. Colloid. Interf. Sci.* 351 (2010) 293.
- [36] A. D. Paolai, M. Bellardita, L. Palmisano, *Catalysts.* (2013) 36.
- [37] T. Kandiel, L. Robben, A. Alkaim, D. Bahnemann, *Photochem. Photobiol. Sci.* 12 (2013) 602.
- [38] G. Bandekar, N. S. Rajurkar, I. S. Mulla, U. P. Mulik, D. P. Amalnerkar, P. V. Adhyapak, *Appl. Nanosci.* 4 (2013) 199.
- [39] J. Gu, Y. Li, W. Li, J. Shi, *Res. Chem. Intermed.* 35 (2009) 807.
- [40] P. V. Viet, B. T. Phan, C. M. Thi, L. V. Hieu, *J. Nanosci. Nanotech.* 16 (2016) 1.
- [41] B. Yu, K. M. Leung, Q. Guo, W. M. Lau, J. Yang, *Nanotech.* 22 (2011) 1.
- [42] Y. H. Liou, S. L. Lo, W. H. Kuan, C. J. Lin, S. C. Weng, *Water Res.* 40 (2006) 2485.
- [43] T. An, J. Liu, G. Li, S. Zhang, H. Zhao, X. Zeng, et al., *Appl. Catal. A.* 350 (2008) 237.
- [44] S. Agarwala, M. Kevin, S. W. Wong, C. K. N. Peh, V. Thavasi, G. W. Ho, *ACS Appl. Mater. Interfaces.* 2 (2010) 1844.
- [45] R. Delaigle, M. M. F. Joseph, D. P. Debecker, P. Eloy, E. M. Gaigneaux, *Top Catal.* 56 (2013) 1867.
- [46] A. Veres, J. Ménesi, A. Juhász, O. Berkesi, N. Ábrahám, G. Bohus, et al., *Colloid. Polym. Sci.* 291 (2014) 207.
- [47] C. Ortiz, R. Torres, D. Paredes, *Int. J. Nanomedicine.* 9 (2014) 1717.
- [48] Z. V. Quiñones-jurado, M. A. Waldo-mendoza, H. M. Aguilera-bandin, E. G. Villabona-leal, E. Cervantes-gonzález, E. Pérez, *Mater. Sci. Appl.* (2014) 89.
- [49] A. Tsivadze, G. Ionova, V. Mikhalko, I. Ionova, G. Gerasimova, *Chem. Surf.* **49** (2013) 169.